

Biophysical Journal, Volume 111

Supplemental Information

**Single-Molecule Specific Mislocalization of Red Fluorescent Proteins in
Live *Escherichia coli***

**Harshad Ghodke, Victor E.A. Caldas, Christiaan M. Punter, Antoine M.
van Oijen, and Andrew Robinson**

Supporting Materials and Methods

Cloning

Construction of linker-FP

Fluorescent proteins mKate2 (GeneArt, Life Technologies) (1), YPet(2) (GeneArt, Life Technologies) and mCherry (3) were PCR amplified with primers containing the sequence for the linker (see table) using KOD polymerase (Novagen) using the following cycling conditions: Initial denaturation 95°C for 5 minutes, denaturation 95°C for 15s, annealing at 58°C for 30s and extension at 72°C for 35s (30X), followed by final extension at 72°C for 1 minute. Insert and vector pBAD-myc-HisB (Invitrogen) were both digested with XhoI and XbaI (New England Biolabs) followed by ligation with T4 DNA ligase at 16°C overnight (New England Biolabs) and transformed into E.coli DH5a. Colonies were screened for insertion by PCR, followed by isolation of plasmid and DNA sequencing (GATC biotech).

Primer	Sequence
Linker-mKate2_FW	atc cga gct cga g ATG TCG GCT GGC TCC GCT GCT GGT TCT GGC GAA TTC ATG GTG AGC GAG CTG ATT AAG GAG
Linker-mKate2_Rev	GTT CCT ATT CTC TAG AAA CTA TAG GAA CTT CTC ATC TGT GC
Linker-YPet_FW	atc cga gct cga g ATG TCG GCT GGC TCC GCT GCT GGT TCT GGC GAA TTC ATGTCTAAAGGTGAAGAATTATTCCTACTGGTGTGTGTC
Linker-YPet_Rev	CGA GGG TAT GAA TGA ATT GTA CAA AGA GCT CTA ATC TAG AAA GCT TCG A
pBAD-mCherry1-F	GGATCCGAGCTCATGGTGAGCAAGGGCGAG
pBAD-mCherry1-R	GCATGTTCTAGATTATTACTTGTACAGCTCGTCCATGC

Construction of LacY-mCardinal

mCardinal insert was amplified from pCDNA-mCardinal using the primers containing KasI and XbaI sites using the PCR program as above with annealing temperature of 70°C and extension time of 20s using KOD polymerase. Both, the insert and pBAD-LacY-eYFP (generous gift from J.T.Mika, University of Groningen) were digested with KasI and XbaI (New England Biolabs) followed by gel purification and ligation with T4 DNA ligase at 16°C overnight. Colonies were screened for the presence of mCardinal (as opposed to eYFP) by digestion of purified plasmid DNA with PstI (New England Biolabs) followed by sequencing.

Primer	Sequence
LacY-mCardinal_F	GGCACTGGAGGCGCC atggtgagcaagggcg
LacY-mCardinal_R	GAGTTTTTGTCTAGA ttactgtacagctcgtccatgc

Preparation of cells for imaging

MG1655 cells carrying pBAD plasmids containing the genes for either linker-mKate2, linker-YPet or mCardinal were cultured overnight at 37°C in EZ rich media (Teknova) with glycerol as the carbon source, and the indicated amounts of L-arabinose, and ampicillin. Overnight cultures were reset in fresh EZ media with glycerol with a 1:100 dilution and grown for at least two hours before imaging. Early log phase cells (OD ~ 0.2) were then sandwiched between a silanized glass cover slip and a

clean cover slip, followed by imaging. Each sample was imaged within 10 minutes of preparation. Coverslips were prepared by first sonicating in 5M KOH for 1 h followed by extensive washing with water. Silanization was performed with 2% 3-aminopropyl triethoxy silane in acetone followed by extensive washing with water and drying with nitrogen.

LacY-mCardinal cells were grown at 37°C in EZ rich media with glycerol as carbon source. Cells were fixed by pelleting an early log phase culture followed by resuspension in 100 mM MgSO₄ and either 2.8% formaldehyde and 0.04% glutaraldehyde for 30 min or 5.6% formaldehyde and 0.08% glutaraldehyde for 15 min. This was followed by washing twice with 100 mM MgSO₄ followed by resuspension in EZ media with glycerol. Resuspended fixed cells were then imaged using the same protocol as for live cells.

Chromosomal fusion of dnaQ-YPet was created by recombination of the YPet-FRT-Kan-FRT cassette into the C-terminus of the dnaQ gene in MG1655 as described previously(4, 5).

Imaging

Samples were imaged on a custom built live-cell imaging microscope (Olympus IX-81) with a 1.49 NA objective and 512x512 pixel² EM-CCD camera (C9100-13, Hamamatsu) with either the 514 nm or 568 nm laser (Sapphire LP, Coherent). Images were acquired under rapid acquisition mode with the first frame being a bright field image followed by rapid acquisition in the fluorescence channel of a total of 500 frames (mKate2 and mCardinal; Emission filter: 645/75 nm) and 400 frames (Ypet; Emission filter: 540/30 nm) with an integration time of 34 ms. mKate2 was imaged at a laser power of 180 Wcm⁻², mCherry and mCardinal were imaged at 18-180 Wcm⁻², whereas YPet was imaged at a laser power of 9 Wcm⁻².

Image analysis and peak detection

Image analysis was performed in ImageJ (6) and Fiji (7) using custom plugins and macros (available at <https://github.com/SingleMolecule>, (8)). Images were processed as follows:

1. The fluorescent channel acquisition was first ‘flattened’ to correct the intensity variation arising from the laser beam profile.
2. Flattened images were then Z-projected to obtain the average projection for each acquisition. These averaged projections were used in conjunction with the brightfield images in MicrobeTracker (9) to identify the cell outlines to identify cells that are in focus.
3. Next, peaks were identified in the flattened acquisitions using custom written ImageJ plugins (8). Acquisitions were first averaged to enhance peaks using the peak filter described in ref (10). These peaks were detected using a fluorophore specific signal-to-noise ratio threshold over the cover-slip background, with a minimum distance between adjacent detected peaks of 3 pixels (100 nm/pixel) in each frame. The following SNRs were used: mKate2: 6, LacY-mCardinal:1, Ypet:5, mCherry:5. This method of peak detection is more sensitive to detecting peaks in cells imaged under single molecule imaging conditions, typically with low fluorophore copy numbers, and hence low cytosolic fluorescence, as opposed to imaging cells with high fluorophore copy numbers.
4. Given the shape of the *E.coli* cell, under conditions of high cytosolic fluorescence, the peak detection algorithm falsely detects fluorescence as broad peaks. To eliminate these false-positives, the peak list thus obtained was filtered to include only peaks that possess a full-width at half maximum height of less than 3 pixels or 330 μm. Additionally, foci that lived for longer than 10 consecutive frames were ignored.

- The peak list was then processed using MicrobeTracker to obtain the relative positions of these peaks within the corresponding cell outline. This peak list consisted of positions (x_i, y_i) for the i^{th} peak such that $x_i \in [-D, D]$ and $y_i \in [0, L]$ where L represents the length of a cell, and $2D$ corresponds to the width of the cell. In this transformation, $(0,0)$ is assigned to one pole of the cell. For purposes of illustration, the cell length was normalized to 50 pixels. For MG1655, mKate2, mCardinal and LacY-mCardinal data, short-axis distributions (Fig 1 and SI Fig1) were obtained by plotting histograms of x_i values for $y_i \in [10, 40]$ to minimize signal from the poles. For ϵ -Ypet, short-axis distributions were obtained by plotting histograms of x_i for the entire range $y_i \in [0, 50]$. Short axis distribution histograms were normalized for number of cells measured.

Calculation of number of molecules in a cell as a function of L-arabinose

The average total intensity of a single fluorophore mKate2 molecule was calculated by plotting a histogram of total intensity of a single peak for peaks detected in the 0% arabinose experiment. This histogram was found to fit a sum of two Gaussians with centers at $4.271e+04$ ($4.102e+04, 4.44e+04$) and $7.745e+04$ ($6.332e+04, 9.159e+04$) (R-square: 0.946) (Figure S1A). Of these, the peak with the lower intensity was assigned to monomeric mKate2. The number of fluorophores in each cell was then calculated by dividing the total cellular fluorescence calculated in each cell (corrected for background) by the total intensity of a single fluorophore as obtained from the fit to the histogram. Calculated this way, the average number of molecules for $0, 5 \times 10^{-3}$ and 10^{-1} percent L-arabinose are $20 \pm 8, 65 \pm 39, 158 \pm 116$ (average \pm std. dev) respectively.

Figure legends:

Figure S1

A. Histogram of mean pixel intensity of mKate2 fluorescence in cells as a function of L-arabinose concentration ($0, 5 \times 10^{-3}$ and 10^{-1} %) **B.** Histogram of total intensity of mKate2 peaks detected in the 0% ara dataset (bars) and fit to distribution with two gaussian terms and **C.** Histogram of number of molecules per cell in mKate2 expressing cells for varying amounts of arabinose ($0, 5 \times 10^{-3}$ and 10^{-1} %).

Figure S2

Bright field, averaged projections of fluorescent acquisitions, reconstructions of the localizations and normalized short-axis distribution of **A.** MG1655 in the red channel ($n_{\text{cells}} = 34, n_{\text{peaks}} = 282$). **B.** YPet expressed under an arabinose promoter in the presence of the indicated concentrations of L-arabinose ($n_{\text{cells}} = 61, 51, 55, 97$ and $95; n_{\text{peaks}} = 2934, 3540, 5885, 9604$ and 9949 for % L-arabinose = $0, 10^{-3}, 5 \times 10^{-3}, 10^{-2}$ and 10^{-1} respectively) **C.** mCardinal expressed under a pBAD promoter in the presence of either 0 % L-arabinose ($n_{\text{cells}} = 51, n_{\text{peaks}} = 1369$) **D.** mCherry (% L-arabinose = $0, n_{\text{cells}} = 33, n_{\text{peaks}} = 635$). Scale bar is $2 \mu\text{m}$. Note that intensities of the peaks in the reconstructions are optimized for display purposes and do not reflect the number of cells measured, whereas short-axis distribution histograms are normalized for the number of cells measured with the same scale as in Fig 1A.

Figure S3

Plot of mean background corrected pixel intensity of mKate2 in cells averaged over the population vs. frame (black trace) and histogram of number of peaks detected as a function of frame (grey trace) for L-arabinose **A.** 0, **B.** 5×10^{-3} and **C.** 10^{-1} percentage in growth medium.

Movie 1

Video of peak enhanced acquisitions showing dynamic nature of mKate2 foci in cells. Foci appear to diffuse along the cell membrane as indicated by the arrows. Each slice in the movie represents a 34 ms exposure, relayed at 10 fps here.

Supporting References

1. Shcherbo, D., C. S. Murphy, G. V. Ermakova, E. A. Solovieva, T. V. Chepurnykh, A. S. Shcheglov, V. V. Verkhusha, V. Z. Pletnev, K. L. Hazelwood, P. M. Roche, S. Lukyanov, A. G. Zaraisky, M. W. Davidson, and D. M. Chudakov. 2009. Far-red fluorescent tags for protein imaging in living tissues. *The Biochemical journal* 418:567-574.
2. Nguyen, A. W., and P. S. Daugherty. 2005. Evolutionary optimization of fluorescent proteins for intracellular FRET. *Nat Biotechnol* 23:355-360.
3. Doherty, G. P., M. J. Fogg, A. J. Wilkinson, and P. J. Lewis. 2010. Small subunits of RNA polymerase: localization, levels and implications for core enzyme composition. *Microbiology* 156:3532-3543.
4. Huang, L. C., E. A. Wood, and M. M. Cox. 1997. Convenient and reversible site-specific targeting of exogenous DNA into a bacterial chromosome by use of the FLP recombinase: the FLIRT system. *J Bacteriol* 179:6076-6083.
5. Reyes-Lamothe, R., D. J. Sherratt, and M. C. Leake. 2010. Stoichiometry and architecture of active DNA replication machinery in *Escherichia coli*. *Science* 328:498-501.
6. Schneider, C. A., W. S. Rasband, and K. W. Eliceiri. 2012. NIH Image to ImageJ: 25 years of image analysis. *Nat Methods* 9:671-675.
7. Schindelin, J., I. Arganda-Carreras, E. Frise, V. Kaynig, M. Longair, T. Pietzsch, S. Preibisch, C. Rueden, S. Saalfeld, B. Schmid, J. Y. Tinevez, D. J. White, V. Hartenstein, K. Eliceiri, P. Tomancak, and A. Cardona. 2012. Fiji: an open-source platform for biological-image analysis. *Nat Methods* 9:676-682.
8. Caldas, V. E., C. M. Punter, H. Ghodke, A. Robinson, and A. M. van Oijen. 2015. iSBatch: a batch-processing platform for data analysis and exploration of live-cell single-molecule microscopy images and other hierarchical datasets. *Molecular bioSystems*.
9. Sliusarenko, O., J. Heinritz, T. Emonet, and C. Jacobs-Wagner. 2011. High-throughput, subpixel precision analysis of bacterial morphogenesis and intracellular spatio-temporal dynamics. *Mol Microbiol* 80:612-627.
10. Hedde, P. N., J. Fuchs, F. Oswald, J. Wiedenmann, and G. U. Nienhaus. 2009. Online image analysis software for photoactivation localization microscopy. *Nat Methods* 6:689-690.

Figure S1

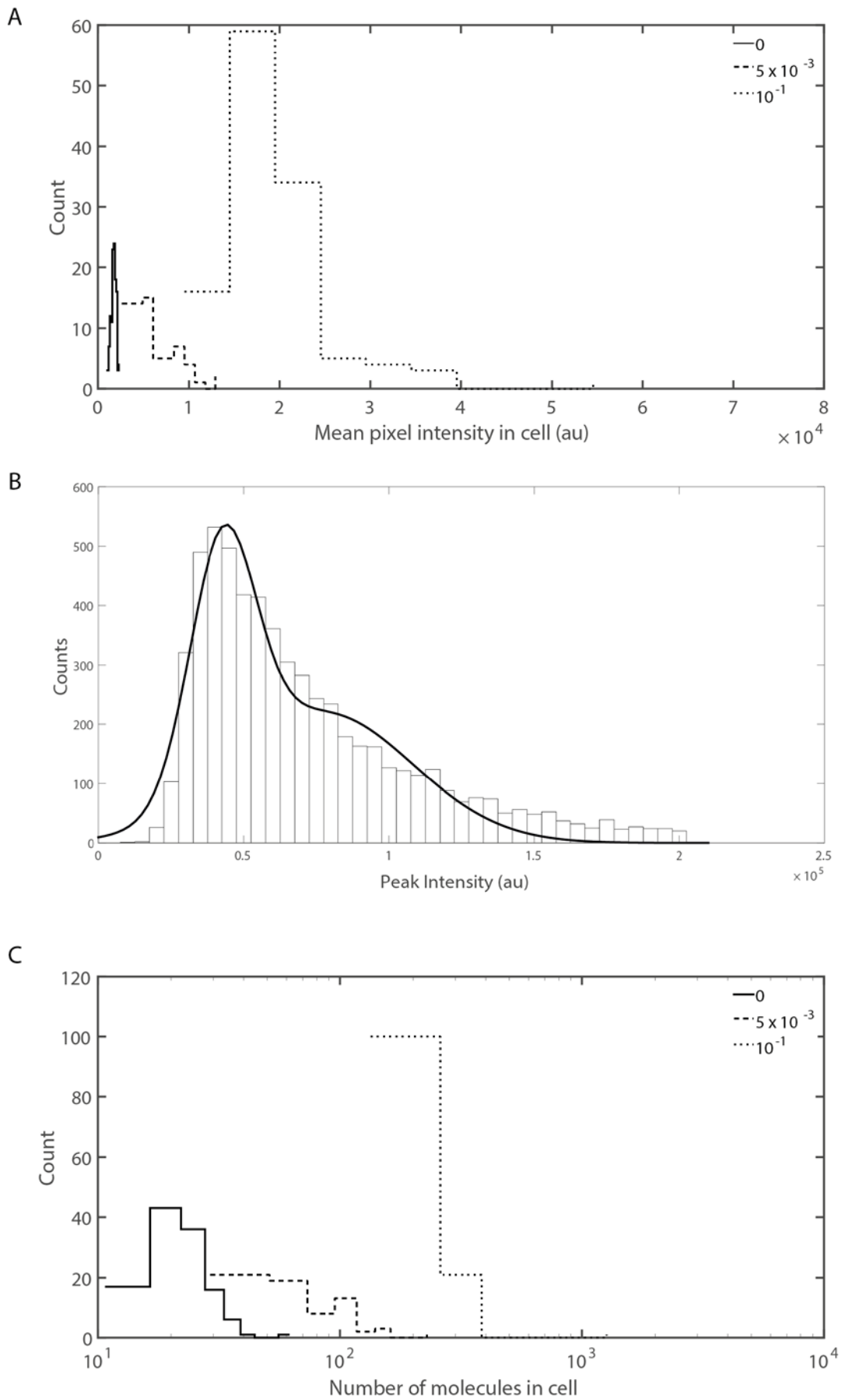


Figure S2

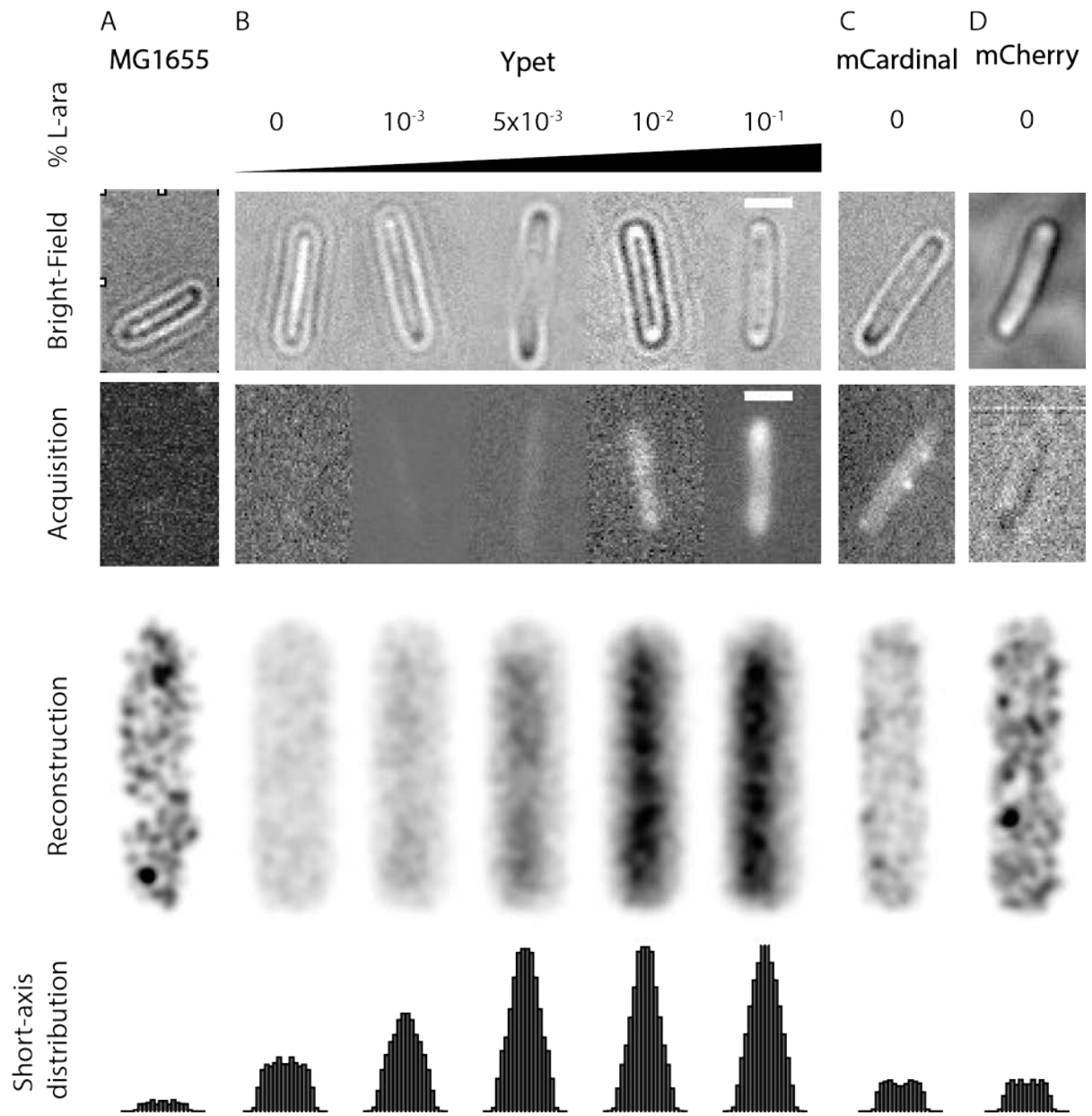


Figure S3

